

Empirical Directional Wave Spectra for Computer Graphics

Christopher J. Horvath*
Google, Inc.



Figure 1: A stormy ocean synthesized with our model and rendered interactively in OpenGL.

Abstract

In this paper, we describe the practical application of several empirically-based, directional ocean wave spectra for use in the Fourier synthesis of animated ocean height fields. We use the Texel MARSEN ARSLOE (TMA) empirical model for the non-directional component of the wave spectrum, and compare a selection of empirically-based directional spreading functions. Additionally, we introduce a novel, normalized parameter called “swell” which modifies the directional spreading to produce wavelength-dependent elongation of waves into parallel wave trains.

This paper builds upon the spectral ocean synthesis techniques popularized for computer graphics in Jerry Tessendorf’s popular SIGGRAPH Course, “Simulating Ocean Water” and the accompanying course notes. The advancement of our spectra over the spectrum described by Tessendorf is that it readily gives plausible, attractive results for a wide range of wind speeds, ocean depths, and other physical parameters, without requiring artists to manually adjust gain and filter parameters to compensate for model inaccuracies. Our “swell” parameter additionally provides an intuitive interface for smoothly varying between choppy seas due to local storms and swells from distant weather events.

CR Categories: I.3.5 [Computer Graphics]: Computational Geometry and Object Modeling—Physically based modeling;

Keywords: ocean simulation, texel marsen arsloe spectrum, direc-

tional spreading function, fourier synthesis, tessendorf waves

1 Introduction

In his 2001-2004 SIGGRAPH Course, “Simulating Ocean Water”, [Tessendorf 2001], Jerry Tessendorf described a methodology for the random generating of time-varying ocean height fields. The technique begins by using a wave spectral density function (wave spectrum) and a gaussian pseudo-random number generator to create an initial state representation in 2D spectral space.

This initial spectral state is propagated forward in time using a relationship between wavelength and wave travel speed (phase velocity) called the dispersion relationship. Finally, the Inverse Fast Fourier Transform is used to convert this propagated spectral representation into 2D height fields, horizontal displacement maps, and crest maps.

This methodology produces beautiful ocean surfaces and is so widely used that these waves are commonly known simply as, “Tessendorf Waves”. The model is supported in a wide variety of commercial and proprietary ocean simulation toolkits, including the popular open source *aaOcean Suite*, which provides plugins for Softimage, Maya, Houdini, Mental Ray, and Arnold. [Akram 2015]. Tessendorf Waves have even been made into fine

Permission to make digital or hard copies of all or part of this work for personal or classroom use is granted without fee provided that copies are not made or distributed for profit or commercial advantage and that copies bear this notice and the full citation on the first page. Copyrights for components of this work owned by others than ACM must be honored. Abstracting with credit is permitted. To copy otherwise, or republish, to post on servers or to redistribute to lists, requires prior specific permission and/or a fee.

Request permissions from Permissions@acm.org.

DigiPro ’15, August 8, 2015, Los Angeles, California.

© 2015 ACM. ISBN 978-1-4503-3718-2/15/08...\$15.00

DOI: <http://dx.doi.org/10.1145/2791261.2791267>

* e-mail: black.encino+waves@gmail.com

dinner-ware: <http://www.allenhemberger.com/alinea/2013/05/tessendorf-plate/>

Challenges of the Tessendorf Model in Practice

Due to the ubiquity of Tessendorf Waves, water simulation visual effects artists have a great deal of experience in shaping the model to achieve realistic ocean scenes, and over time have identified challenging aspects. While it is true that different implementations of the model have presented tools for lessening these difficulties, they are largely informal and unpublished. Therefore, in this paper we restrict our analysis and improvements to the model as originally published. Here is a list of some of the primary difficulties:

- **Amplitude Tuning:** The amplitude gain of the model is not explicitly provided. It has to be set visually, and tends to need different settings for different ocean categories, such as calm seas vs. raging storms. While it is true that an implementation can normalize the model to a good initial value, this is nonetheless an area that involves frequent parameter tuning.
- **Spectrum Accuracy:** Plainly speaking, it is challenging to create an aesthetically pleasing ocean surface with the model without combining several wave fields and without the use of filters. Less subjectively, the directional and non-directional spectra used in the model are a poor empirical fit to observed ocean behavior. [Ochi 1998]. The model tends to produce waves evenly across the range of wavelengths, whereas visual references show a more pronounced concentration of wave energy in peak wavelengths, increasingly so as sea severity increases. The excessive middle-wavelength energy often leads artists to use band-pass filters to isolate desired wavelengths, and to combine multiple wave fields to sculpt a desired look. The parameter-tuning of such filters is difficult, involving usually at least three parameters per filter, and when multiple wave fields are combined, each new wave field has a completely independent set of parameters. This can quickly lead to confusion as effects from one set of waves interfere with those from another set.
- **Shallow Water:** The model doesn't adjust wave amplitudes to account for shallow ocean depths. While this can be partially ameliorated by lowering the amplitude gain manually, doing so dampens all wavelengths equally, whereas the effects of shallow water should be more pronounced on larger waves.
- **Directional Spreading:** The directional spreading model is a fixed, unparameterized falloff that is the same for all wavelengths. Without modification, it is impossible to create long swells, and even with modification, the distribution of perpendicular waves is difficult to get exactly correct.

In this paper, we address these areas of difficulty by demonstrating the practical application of the Texel MARSEN ARSLOE (TMA) non-directional wave spectrum and a selection of empirically-based directional spreading functions including the Mitsuyasu and Hasselmann models. The TMA model is easy for artists to use, and dramatically cuts down on the amount of tuning and expertise required to achieve a plausible ocean that matches a reference. The TMA model is empirical, essentially a high-order curve fit to an extremely large set of measured ocean height, wind-speed, fetch, and ocean-depth data. [Hughes 1984; Ochi 1998]

For the directional component of the spectrum, we evaluate several different empirically-based directional spreading functions, each of which has no user-tunable parameters. We compare these to the \cos^2 spreading function used by [Tessendorf 2001]. These models

are based around seas affected by local wind events, and are therefore fairly choppy.

We propose a novel, normalized parameter named “swell”, with a useful range of $[0, 1]$, which allows an artist to smoothly transition from a base wave field with empirical directional spreading to a strongly elongated train of directed, parallel waves. The swell parameter is used to directly modify the directional spreading functions, and can be used with any of the models.

2 Previous Work

The stochastic approach to the study of ocean waves began in the 1950's, when the first wave spectrum models were proposed such as those in [Pierson et al. 1954]. The wave spectrum equilibrium range was first described by [Phillips 1958], and developed into the Pierson-Moskowitz spectrum in [Pierson and Moskowitz 1964]. The JONSWAP spectrum we use in this paper was developed by [Hasselmann et al. 1973]. Using the work of [Kitaigorodskii et al. 1975], [Bouws 1985a] created the Texel MARSEN ARSLOE (TMA) spectrum, which was again elaborately studied by [Hughes 1984]. The directional spreading functions we examine were developed by [Longuet-Higgins et al. 1961], [Mitsuyasu 1975], [Hasselmann et al. 1973], and [Donelan et al. 1985], all based on parameter and model fitting to different ocean wave data sets.

A vast number of research papers and books on the stochastic study of oceans have been, and continue to be published. The topic has great impact on the design and engineering of marine systems. [Ochi 1998] is the book that the majority of the physical oceanography references in this paper began with, and provides an excellent and thorough overview of the subject. We also referred to [Young 1999] for elaboration on fetch and a very in-depth discussion of directional spreading functions. [Stewart 2008] provides a more introductory approach to physical oceanography, and was useful in helping develop an intuitive understanding of the core concepts, particularly the formulation of the spectrum from the Fourier transform. [Wen et al. 1993] provide a different theoretical derivation of a physical directional spreading function, though we eschew their formulation due to its complexity.

Within the realm of computer graphics, there have been many contributions to the creation of ocean wave height fields. [Fournier and Reeves 1986] showed how to combine Gerstner Waves as deformations of patch vertices to produce very realistic breaking waves for that time. [Kass and Miller 1990] demonstrated the solution of the shallow water equations on a 2D height field to generate shallow water waves that are capable of interaction with objects over time. [Tessendorf 2001]'s SIGGRAPH Courses introduced the physical oceanographic approach to synthesized FFT waves, and is the primary work this paper is based upon. Though not related to oceans specifically, the FFT fluid solver presented by [Stam 2002] provided a concise, working solver using the FFT, and became a starting point for many implementations of FFT-based 2D solvers.

Full 3D solutions to the Navier Stokes equations began to be introduced to computer graphics by [Foster and Metaxas 1996], and have been aggressively improved upon since then. Despite significant advancements, though, full 3D solutions for deep oceans still use height fields as a base layer, or as a boundary condition, or as a guide shape. [Nielsen and Bridson 2011]. In [Nielsen et al. 2013], the authors create a system capable of inverting an existing height field into the best fit parameters to the ocean model from [Tessendorf 2001]. Their method is specific to that model, though we hope this paper will encourage an adaptation to a new set of parameters.

The FFT, or Fast Fourier Transform, was originally described by [Cooley and Tukey 1965], though the method actually dates back to Gauss. Many current implementations of FFT ocean solvers rely on the FFTW (Fastest Fourier Transform in the West) library from MIT. The implementation of FFTW3 is described by its authors in [Frigo and Johnson 2005].

Lastly, a presentation of the TMA spectrum appeared in [Lee et al. 2008], with a directional spreading function that is similar to the Mitsuyasu model we present in this paper.

3 Nomenclature and Basic Relationships

Symbol	Meaning
λ	Wavelength
T	Period
ω	Angular Frequency
f	Ordinary Frequency
θ	Angle of wave relative to wind direction
$S(\omega, \theta)$	Wave spectrum
$S(\omega)$	Non-directional Wave Spectrum
$D(\theta)$	Directional Spreading Function
\mathbf{k}	Wave number vector, or Wave vector
k_x	X component of Wave vector
k_y	Y component of Wave vector
k	Magnitude of wave vector
$\omega = \phi(k)$	Dispersion Relationship
E	Time average of wave energy
ρ	Density of water = 1000
σ	Surface Tension coefficient = 0.074
g	Gravitational constant = 9.81
h	Ocean depth
U	Average wind speed
F	Fetch
a	Wave amplitude
t	Time
ξ	Swell

Table 1: Nomenclature and Symbols

The spectra presented in this paper rely on a large number of physical parameters and different variables. Table 1 lists the symbols we use along with their meanings. The definition of some of these physical properties in terms of each other are given by the following definitive equations:

$$\omega = \frac{2\pi}{T} \quad (1)$$

$$\omega = 2\pi f \quad (2)$$

$$\mathbf{k} = (k_x, k_y) \quad (3)$$

$$k = \sqrt{k_x^2 + k_y^2} \quad (4)$$

$$k = \frac{2\pi}{\lambda} \quad (5)$$

$$\theta = \arctan \frac{k_y}{k_x} \quad (6)$$

4 Wave Dispersion

In order to discuss the wave spectra in detail, we must first present a functional relationship between the travel speed of waves and their wavelengths. This relationship is called the dispersion relationship, and is written as a function relating angular frequency ω to the wave number k . The dispersion relationships depend on gravity, ocean depth, and other physical parameters.

A simple discussion and derivation of dispersion relationships is given in [Read 2009]. For deep water, in which the ocean depth is vastly larger than considered wavelengths, the dispersion relationship is derived as:

$$\omega^2 = gk \quad (7)$$

A finite-depth dispersion relationship is:

$$\omega^2 = gk \tanh kh \quad (8)$$

Where h represents the ocean depth.

We can include a term which will only influence the relationship when waves have very small wavelengths, to simulate capillary wave dispersion. Capillary waves are small waves, typically with wavelengths less than a few centimeters, whose dynamics are primarily governed by surface tension. A dispersion relationship which incorporates the effects of surface tension at small scales as well as the full effects of gravity and ocean depth is:

$$\omega^2 = (gk + \frac{\sigma}{\rho} k^3) \tanh kh \quad (9)$$

where σ represents the surface tension coefficient in units of N/m, and ρ represents the density in kg/m^3 . These relationships are all approximations, and there is a large set of different relationships to choose from. See the Wikipedia entry [https://en.wikipedia.org/wiki/Dispersion_\(water_waves\)](https://en.wikipedia.org/wiki/Dispersion_(water_waves)) for many more.

The capillary formulation given in (9) is nearly identical to the finite depth formulation given in (8) for waves with large wavelengths, for which the $\frac{\sigma}{\rho} k^3$ term approaches zero. Similarly, the finite depth formulation is nearly identical to the deep water formulation in (7) for large wavelengths when $\tanh kh$ approaches unity. Therefore, we always use the capillary formulation in our implementation. For mathematical analysis, though, we may resort to either the Deep or Finite Depth representations as the need for simplification demands.

5 The Wave Spectrum

The wave spectral density function, or wave spectrum, is a function which expresses the time-average energy of a random ocean configuration as a continuous function of angular frequency ω and direction θ . Spectral analysis of a height field represents the field as an infinite sum of discrete 2d cosine waves.

A single 2D wave in an XYZ cartesian coordinate system, with Z up, can be described by the following equation:

$$\eta_i(x, y, t) = a_i \cos \left[k_i (\cos \theta_i + \sin \theta_i) - \omega_i t + \epsilon_i \right] \quad (10)$$

where a is an amplitude, ω is the angular frequency of the wave, k is the wavenumber, θ is the direction of the wave counterclockwise from the positive x-axis, t is time, and ϵ is the phase offset. Using vector notation,

$$\begin{aligned} \mathbf{r} &= (x, y) \\ \mathbf{k}_i &= (k_i \cos \theta_i, k_i \sin \theta_i) \\ &= (k_{xi}, k_{yi}) \\ \eta_i(\mathbf{r}, t) &= a_i \cos(\mathbf{k}_i \cdot \mathbf{r} - \omega_i t + \epsilon_i) \end{aligned} \quad (11)$$

Because ω and θ are both functions of \mathbf{k} , a single wave is characterized entirely by the numbers $(\mathbf{k}_i, a_i, \epsilon_i)$. The entire ocean surface is then just a sum of infinitely many of these 2D waves:

$$\eta(\mathbf{r}, t) = \sum_{i=0}^{\infty} a_i \cos(\mathbf{k}_i \cdot \mathbf{r} - \omega_i t + \epsilon_i) \quad (12)$$

For each of the infinitely many discrete waves η_i , there is an infinitesimally small interval of the spectral domain defined as $[\omega_i, \omega_i + \Delta\omega_i]$, $[\theta_i, \theta_i + \Delta\theta_i]$, and the amplitude contribution a_i is also infinitesimally small. We can formally define the wave spectrum now in a useful form that will allow us to relate the spectrum to amplitudes in spectral space:

$$\sum_{\Delta\omega_i} \sum_{\Delta\theta_i} \frac{a_i^2}{2} = \int_{-\pi}^{\pi} \int_0^{\infty} S(\omega, \theta) d\omega d\theta \quad (13)$$

We can write equation (13) over only the i^{th} interval as:

$$\frac{a_i^2}{2} = \int_{\theta_i}^{\theta_i + \Delta\theta_i} \int_{\omega_i}^{\omega_i + \Delta\omega_i} S(\omega, \theta) d\omega d\theta \quad (14)$$

which can be discretely approximated:

$$\frac{a_i^2}{2} \approx S(\omega_i, \theta_i) \Delta\omega_i \Delta\theta_i \quad (15)$$

Each distinct random ocean surface has one and only one spectrum associated with it, and just as each surface is unique, each spectrum is unique. The different spectral models we discuss below in detail are intended to represent the average over a very large number of unique random oceans with the same physical characteristics.

The directional wave spectrum $S(\omega, \theta)$ is written as the product of a non-directional spectrum $S(\omega)$ and a directional spreading function $D(\omega, \theta)$:

$$S(\omega, \theta) = S(\omega)D(\omega, \theta) \quad (16)$$

We present independent models for each component, starting with the non-directional spectra.

5.1 Non-Directional Wave Spectra

[Phillips 1958] introduced the notion of a “fully developed ocean”, in which wind blew over a very large region of the ocean, significantly larger than the wavelengths being considered, for a long enough time that the waves reach equilibrium with the wind. In such an equilibrium state, no additional energy is transferred from the wind to the waves, and the ocean is “fully developed”. This is intuitively analogous to pushing a swing at the same speed that it is already moving. From [Hughes 1984]:

Phillips suggested that there should be a region of the wind-generated deepwater gravity waves in which the wave energy density has an upper bound given by the following expression:

$$E_{\text{Phillips}}(\omega) = \alpha 2\pi \frac{g^2}{\omega^5} \quad (17)$$

5.1.1 The Pierson-Moskowitz Spectrum

[Pierson and Moskowitz 1964] used data gathered from British weather ships in the North Atlantic to empirically determine coefficients for a spectrum function based on the Phillips equilibrium range. [Stewart 2008; Ochi 1998; Pierson and Moskowitz 1964] The spectrum they developed for representing fully-developed seas is:

$$\begin{aligned} S_{\text{PiersonMoskowitz}}(\omega) &= \frac{\alpha g^2}{\omega^5} \exp(-\beta(\frac{\omega_0}{\omega})^4) \quad (18) \\ \alpha &= 8.1 \times 10^{-3} \\ \beta &= 0.74 \\ \omega_0 &= g/(1.026U) \end{aligned}$$

The peak frequency, ω_p , is the angular frequency for which the waves have the most average energy, and for this spectrum is calculated as:

$$\omega_p = 0.855g/U \quad (19)$$

5.1.2 The Generalized A,B Spectrum

[Ochi 1998] lists a number of wave spectra that have the same form as Pierson-Moskowitz, differing only in their constant coefficients.

$$S_{\text{A,B}}(\omega) = \frac{A}{\omega^5} \exp(-\frac{B}{\omega^4}) \quad (20)$$

The Pierson-Moskowitz Spectrum can be described as an A,B Spectrum with $A = \alpha g^2$ and $B = \beta \omega_0^4 = 0.6858(g/U)^4$.

5.1.3 The Tessendorf Spectrum

The full directional spectrum used in [Tessendorf 2001] is described as a wave number spectrum $S(\mathbf{k})$:

$$S_{\text{Tessendorf}}(\mathbf{k}) = A_T \frac{\exp(-\frac{g^2}{U^4}/k^2)}{k^4} D(\mathbf{k}) \quad (21)$$

Where A_T is a user-provided scaling factor. To convert this into the $S(\omega, \theta)$ form that we use for the other spectra in this paper, we'll work backwards from the A,B Spectrum. Using the simple deep water dispersion relationship $\omega = \sqrt{gk}$, we can substitute the wave number spectrum formulation from equation (61) derived in the appendix, into the A,B Spectrum from equation (20), using the full directional form from equation (16). Starting with equation (61) with (16) substituted:

$$S(\mathbf{k}) = S(\omega)D(\omega, \theta) \frac{\partial\omega}{\partial k}/k$$

and the dispersion relationship with its derivative:

$$\omega = \sqrt{gk} \quad (22)$$

$$\frac{\partial\omega}{\partial k} = \frac{g}{2\sqrt{gk}} \quad (23)$$

then substituting the A,B Spectrum from equation (20), and simply writing the directional component as D

$$S(\mathbf{k}) = \frac{A_{ab}}{(gk)^{5/2}} \exp(-\frac{B_{ab}}{(gk)^2})(\frac{g}{2\sqrt{gk}}/k)D \quad (24)$$

Combining terms, we get:

$$S(\mathbf{k}) = (\frac{A_{ab}}{2g^2}) \frac{\exp(-\frac{B_{ab}}{g^2}/k^2)}{k^4} D \quad (25)$$

This is exactly the form of the Tessendorf Spectrum given in (21), so we can say that the non-directional part of the Tessendorf Spectrum is an A,B Spectrum with coefficients:

$$A_{ab} = 2A_T g^2 \quad (26)$$

$$B_{ab} = (g/U)^4 \quad (27)$$

Given that A_T is unspecified, the Tessendorf Spectrum is nearly identical to the Pierson-Moskowitz spectrum, differing only in a multiplier of 0.6858 on the coefficient B, or alternatively, a 1.0989 multiplier on the wind speed U . [Ochi 1998] describes the relationship of wind speeds measured at different height z above the water

level in terms of the wind speed U_{10} at 10 meters above the water level as follows:

$$\begin{aligned} U_z &= U_{10} + u_* \ln(z/10) \\ u_* &= \sqrt{C_{10}} U_{10} \\ C_{10} &= (0.8 + 0.065U_{10})x10^{-5} \end{aligned}$$

Rearranging terms, we can write the relationship between U_z and U_{10} as a multiplier:

$$\frac{U_z}{U_{10}} = 1 + \sqrt{C_{10}} \ln(z/10)$$

This overlooks the dependence of the C_{10} term on U_{10} , but the larger point remains that the ultimate difference between the Tessendorf Spectrum and the Pierson-Moskowitz Spectrum amounts to essentially a very minor variation in the measured average wind speed, which could be accounted for a difference in measurement height. The research bears this out, given that [Phillips 1958] uses wind speed at 10 meters, but [Pierson and Moskowitz 1964] uses wind speed measured at 19.5 meters. Another possible interpretation for the slight coefficient difference is that we used the deep water dispersion relationship (7) rather than the finite depth dispersion relationship (8). We can therefore assert that the Tessendorf Spectrum is essentially identical to the Pierson-Moskowitz Spectrum. In our implementation, we use the A,B Spectrum for both cases to allow for comparison, but there is essentially no visible difference between the two.

Tessendorf advises that his spectrum by itself has “poor convergence properties for high values of k ”, and advises damping out small scale waves and multiplying the final spectrum by the factor $\exp(-k^2 l^2)$, for a user-provided small wavelength $l \ll L$. This bears some resemblance to the peak amplification features of the JONSWAP Spectrum, which is empirically based and not bound to a tuning parameter l .

5.1.4 The JONSWAP Spectrum

Based on analysis of data collected as part of the Joint North Sea Wave Observation Project (JONSWAP), [Hasselmann et al. 1973] found that the oceans never reach a fully-developed state. Non-linear interactions between waves, breaking of large wave crests, directional diffusion of wave energy, and turbulence in the wind itself all contribute to the continued development of waves. As described in [Stewart 2008],

Hence an extra and somewhat artificial factor was added to the Pierson-Moskowitz spectrum in order to improve the fit to their measurements. The JONSWAP spectrum is thus a Pierson-Moskowitz spectrum multiplied by an extra peak enhancement factor γ^r

The JONSWAP spectrum is formulated as follows:

$$\begin{aligned} S_{\text{JONSWAP}}(\omega) &= \frac{\alpha g^2}{\omega^5} \exp\left(-\frac{5}{4}\left(\frac{\omega_p}{\omega}\right)^4\right) \gamma^4 & (28) \\ r &= \exp\left(-\frac{(\omega - \omega_p)^2}{2\sigma^2 \omega_p^2}\right) \\ \alpha &= 0.076 \left(\frac{U^2}{Fg}\right)^{0.22} \\ \omega_p &= 22 \left(\frac{g^2}{UF}\right) \\ \gamma &= 3.3 \\ \sigma &= \begin{cases} 0.07 & \omega \leq \omega_p \\ 0.09 & \omega > \omega_p \end{cases} \end{aligned}$$

Where F is the fetch, which is the length of the area over which the wind is acting on the water, formally defined as “the distance from a lee shore”. The fetch term can be intuitively understood as the abstract size of the wind event over distance and time that is producing the waves. [Young 1999] presents an extremely detailed look at the measurement, geometry, and effects of fetch on wave spectra.

The JONSWAP Spectrum is similar to the Pierson Moskowitz spectrum, but waves continue to grow as distance and time grow (fetch), with a much more pronounced peak. Aesthetically, this means that the primary waves are strongly visible, with other wavelengths relatively damped out. This produces a much better visual match to photographs of ocean states.

5.1.5 The Texel MARSEN ARSLOE (TMA) Spectrum

The JONSWAP Spectrum was fit to observations of waves in deep water. [Kitaigorodskii et al. 1975] studied how deep water spectra could be adapted to match field observations for shallow water equilibrium ranges [Hughes 1984]. They developed a frequency-dependent function of ocean depth which can be applied as a multiplier to a deep water spectrum. This is known as the Kitaigorodskii Depth Attenuation Function, and takes the form:

$$\Phi(\omega_h) = \left[\frac{(k(\omega, h))^{-3} \frac{\partial k(\omega, h)}{\partial \omega}}{(k(\omega, \infty))^{-3} \frac{\partial k(\omega, \infty)}{\partial \omega}} \right] \quad (29)$$

Where ω_h is a dimensionless frequency defined by $\omega \sqrt{h/g}$. This is an intimidating function at first glance, but when plotted as a function of ω_h , as seen in Figure 2, we see that the function takes a very simple shape that we can easily approximate. An approximation for

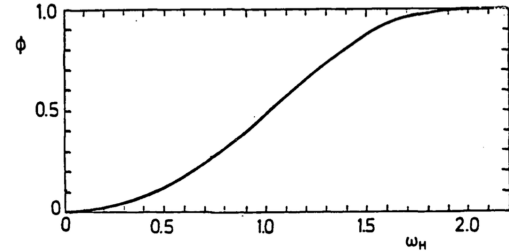


Figure 1. Kitaigorodskii et al.'s Φ as a function of ω_h (Bouws et al. 1985a)

Figure 2: $\Phi(\omega, h)$ as a function of ω_h
[Hughes 1984]

$\Phi(\omega, h)$ given in [Thompson and Vincent 1983] is:

$$\Phi(\omega, h) \approx \begin{cases} \frac{1}{2} \omega_h^2 & \text{if } \omega_h \leq 1 \\ 1 - \frac{1}{2}(2 - \omega_h)^2 & \text{if } \omega_h > 1 \end{cases}$$

This approximation has less than 4% error over the plotted domain [Hughes 1984]. A smoothstep function from 0 to 2.2 or a stretched and translated tanh function will also work.

We quote [Hughes 1984] directly in describing the extent of effort taken to produce the TMA spectral parameterization:

[Bouws 1985a] used field data from three separate studies on shallow-water wind wave growth to investigate the parameters used in the TMA spectral representation. MARSEN (the Marine Remote Sensing Experiment at

the North Sea) and ARSLOE (the Atlantic Remote Sensing Land-Ocean Experiment) were both comprehensive experiments in which ocean wave measurements were but a part of the entire program. The experimental sites are both on the continental shelf with depths up to 40 m; but the ARSLOE site was open to the Atlantic Ocean, while the MARSEN site was located in the southern half of the North Sea. The Texel data set is comprised of a series of measurements made near the Texel lightship west of Rotterdam during a longlasting northwesterly storm in the central and southern North Sea.

The combined data represent conditions with wind-speeds ranging between 4 and 25 m/sec, bottom materials ranging from fine to coarse sands, bottom slopes ranging from 1:150 to nearly flat, and depths from about 5m to 45m.

[Bouws 1985a] fitted the TMA spectral form to over 2,800 wind sea spectra to test its viability and to determine if any parametric relationships could be established linking the spectral parameters to the external wind field. In general the fit of the spectrum was of the same quality as the fit of the JONSWAP spectrum to deepwater wind sea spectra.

Wonderfully, for all the detail and care taken, the final form of the spectrum is just the product of the JONSWAP spectrum and the Kitaigorodskii Depth Attenuation function:

$$S_{\text{TMA}}(\omega) = S_{\text{JONSWAP}}(\omega)\Phi(\omega, h) \quad (30)$$

The incorporation of depth damping alleviates a significant challenge for artists working to create plausible oceans in an environment. Figure 3 shows a somewhat blustery sea state with an ocean depth of 15 meters, for each of the Pierson-Moskowitz, JONSWAP and TMA Spectra. The TMA's waves are damped down and reveal more detail, believably existing in a semi-shallow body of water, whereas the other two look cartoonishly exaggerated.

Figure 3 also illustrates the ease of use of the TMA spectrum in a shallow scene of 15m depth. In this example, the wind speed and ocean depth were set once, and then a camera angle was chosen. If we were using either of the other spectra, we'd have to begin adjusting magnitude gains to get something realistic looking. With TMA the results are believable immediately, in a way that matches the parameters.

6 Directional Spreading

The study of how wave energy disperses directionally, relative to the primary wind direction, is extremely elaborate. From a theoretical perspective, the amount of spreading is a function of energy concentration in a given wavelength, which is related to the notion of the sea's development, and is therefore a function of the primary wind speed, the fetch, and the spectrum. Furthermore, there is a distinction between the directional spreading of the locally affected Sea versus the directional spreading of the Swell, which is wave energy that travels into an area from excitation by wind or storm elsewhere. [Ochi 1998].

The Directional Spreading function is written $D(\omega, \theta)$. It multiplies the non-directional spectrum function $S(\omega)$ to produce the directional spectrum $S(\omega, \theta)$, as shown in equation (16). Any form of $D(\omega, \theta)$ must satisfy the condition:

$$\int_{-\pi}^{\pi} D(\omega, \theta) d\theta = 1 \quad (31)$$

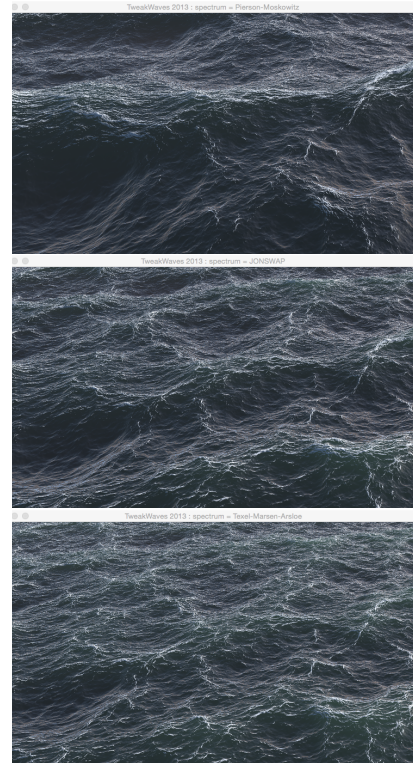


Figure 3: Shallow oceans shown for a 250m patch with 25m/s wind speed, 15m ocean depth, and three different spectra. From top to bottom, the Pierson-Moskowitz, JONSWAP, and TMA Spectra.

6.0.6 Positive Cosine Squared Directional Spreading

[Tessendorf 2001] uses the square of the cosine of θ , which treats waves moving opposite the wind the same as waves moving with the wind. [Ochi 1998] describes the same function but truncated to only the portion of the domain for which the cosine is positive. We call this the Positive Cosine Squared directional spreading function. It does not depend on ω , so it causes all wavelengths to be elongated equally for a given θ .

$$D_{\cos^2}(\theta) = \begin{cases} \frac{2}{\pi} \cos^2(\theta) & \text{if } \frac{-\pi}{2} < \theta < \frac{\pi}{2} \\ 0 & \text{otherwise} \end{cases} \quad (32)$$

This function produces strongly directional waves that all have the same elongation shape. It does not match empirical data, and does not always look right aesthetically, which motivates a need for more robust, empirical models. [Young 1999] provides a detailed discussion of directional spreading, and provides three different models for comparison, which we refer to by their author references: Mitsuyasu, Hasselmann, and Donelan-Banner.

6.0.7 Mitsuyasu Directional Spreading

[Mitsuyasu 1975] fit a directional data set captured with a cloverleaf buoy to a function with a single shaping parameter, s , of a form described in [Longuet-Higgins et al. 1961]:

$$D(\omega, \theta) = Q(s)|\cos(\theta/2)|^{2s} \quad (33)$$

where $Q(s)$ is a normalization factor to satisfy the condition in (31). [Ochi 1998] provides a closed-form approximate solution for $Q(s)$

expressed in terms of the Euler gamma function:

$$Q(s) = \frac{2^{2s-1}}{\pi} \frac{\Gamma(s+1)^2}{\Gamma(2s+1)} \quad (34)$$

The parameter s is fit to the data as follows:

$$s = \begin{cases} s_p(\omega/\omega_p)^5 & \omega \leq \omega_p \\ s_p(\omega/\omega_p)^{-2.5} & \omega > \omega_p \end{cases} \quad (35)$$

where ω_p is the peak angular frequency for the non-directional spectrum, and s_p is calculated from ω_p and physical parameters as follows:

$$s_p = 11.5(\omega_p U/g)^{-2.5} \quad (36)$$

6.0.8 Hasselmann Directional Spreading

[Hasselmann et al. 1973] fit the JONSWAP data set to produce a directional spreading function that also uses the [Longuet-Higgins et al. 1961] form in Equation (33), but with s computed differently:

$$s = \begin{cases} 6.97(\omega/\omega_p)^{4.06} & \omega \leq \omega_p \\ 9.77(\omega/\omega_p)^{-2.33-1.45((U\omega_p/g)-1.17)} & \omega > \omega_p \end{cases} \quad (37)$$

6.0.9 Donelan-Banner Directional Spreading

As referenced in [Young 1999], [Donelan et al. 1985] performed an analysis over a larger set of directional wave data and found the Mitsuyasu/Hasselmann forms inadequate. They proposed an alternative form:

$$D(\omega, \theta) = \frac{\beta_s}{2 \tanh(\beta_s \pi)} \operatorname{sech}(\beta_s \theta)^2 \quad (38)$$

The parameter fit for β_s is elaborate, with the section for $\omega/\omega_p > 1.6$ being a modification added by Banner [Young 1999].

$$\begin{aligned} \beta_s &= \begin{cases} 2.61(\omega/\omega_p)^{1.3} & \text{for } 0.56 < \omega/\omega_p < 0.95 \\ 2.28(\omega/\omega_p)^{-1.3} & \text{for } 0.95 \leq \omega/\omega_p < 1.6 \\ 10^\epsilon & \omega/\omega_p \geq 1.6 \end{cases} \\ \epsilon &= -0.4 + 0.8393 \exp[-0.567 \ln((\omega/\omega_p)^2)] \end{aligned}$$

In our implementation, we use the first case for $\omega/\omega_p < 0.95$, because when we truncate at 0.56 as suggested above, it doesn't have as pleasing of an appearance.

6.0.10 Flat and Mixed Directional Spreading

It is sometimes useful, for aesthetic reasons, to remove directionality entirely. A completely flat directional spreading function, with no shaping at all is simply:

$$D_{flat}(\omega, \theta) = \frac{1}{2\pi} \quad (39)$$

Any two directional spreading functions that meet the constraint in equation (31) can be linearly interpolated to produce a mixed directional spreading function, as follows:

$$D_{mixed}(\omega, \theta) = (1 - \tau)D_A(\omega, \theta) + \tau D_B(\omega, \theta) \quad (40)$$

for some mixing parameter $0 \leq \tau \leq 1$.

6.1 The Swell Parameter

The wave spectra described thus far relate to waves generated by a local source of wind, and the resulting shape of the directional spreading tends to be somewhat choppy, for each of the empirical spreading models described in section 6. It's common for artists to need to create more elongated, parallel waves in certain circumstances. The physical justification for these waves is described by [Ochi 1998] in the following passage:

...the source of irregularity in waves observed in a sea is usually the local wind. Sometimes, however, another wave system, called *swell*, runs across or mixes with wind-generated local waves. Swell is defined as waves which have traveled out of their generating area. During the course of traveling, shorter waves are overtaken by larger waves resulting in a train of more regular long waves moving in its own direction. Fairly large waves observed at sea with minor or even no wind may be categorized as swell.

When swell mixes with the local wind-generated waves, it is not easily identified in the wave record; however, it can be clearly identified in the wave spectrum.

In comparing two actual data sets, one with swell and one without, we can see the presence of the swell as a distinct ocean pattern on top of the base ocean pattern, as seen in Figure 4. We can add the

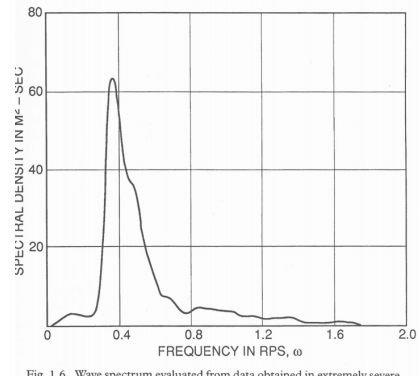


Fig. 1.6. Wave spectrum evaluated from data obtained in extremely severe seas (significant wave height 16.1 m).

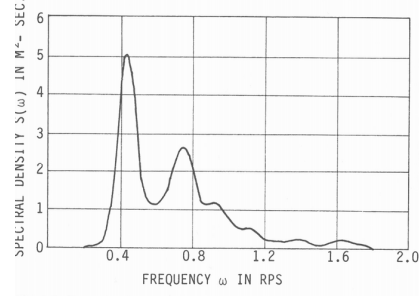


Fig. 1.5. Example of combined swell and wind-generated wave spectrum (significant wave height 4.9 m).

Figure 4: On top, a wave spectrum in severe seas, showing a single pronounced peak. On bottom, a mixed sea and swell spectrum showing two distinct peaks.

[Ochi 1998]

results of two random spectral initial states together to produce a compound spectrum, which will handle the separation of the sea and swell without trying to create a confusing dual parameterization. This can be done within the spectral field synthesis directly,

or as a post-effect on the spatial displacement fields produced by the Inverse FFT. In our formulations here, we've been implicitly assuming that the primary wind direction along the x-axis, that is: $\theta_0 = 0$. It's trivial to add a wind direction bias by simply writing:

$$\theta = \arctan\left(\frac{k_y}{k_x}\right) - \theta_0 \quad (41)$$

We therefore focus our efforts on creating a function of a single "swell" parameter which will control elongation, denoted by the symbol ξ . The parameter should be normalized to the range [0, 1] for the predominant useful range of its effects, and designed such that it feels perceptually linear to a user - meaning that small changes at any part of the domain produce approximately the same visual change.

For the directional spreading functions "out of the box", the waves are concentrated along the wind direction in differing degrees, but always with the peak frequency being the most elongated, except for the cosine squared spreading function, for which all frequencies are equally elongated.

To simulate the effects of swell from a distant wind event, we want to design a function $D_\xi(\omega, \theta)$ which elongates waves increasingly as their wavelengths increase, but asymptotically approaches a maximum elongation. This is in keeping with the description of swell from [Ochi 1998] and also visual references.

The final directional spreading function is defined as:

$$D_{\text{final}}(\omega, \theta) = Q_{\text{final}}(\omega) D_{\text{base}}(\omega, \theta) D_\xi(\omega, \theta) \quad (42)$$

$$Q_{\text{final}}(\omega) = 1 / \left[\int_{-\pi}^{\pi} D_{\text{base}}(\omega, \theta) D_\xi(\omega, \theta) d\theta \right] \quad (43)$$

We use the Longuet-Higgins form from equation (33) as the basis for D_ξ , but compute the s_ξ shaping parameter differently. The hyperbolic tangent function satisfies the property that shaping (elongation) asymptotically increases. The squaring of the parameter ξ produces a perceptual linearization of the parameter. Thus, D_ξ and s_ξ are defined as follows:

$$D_\xi(\omega, \theta) = Q_\xi(s_\xi) |\cos(\theta/2)|^{2s_\xi} \quad (44)$$

$$s_\xi = 16 \tanh\left(\frac{\omega_p}{\omega}\right) \xi^2 \quad (45)$$

where 16 is an entirely subjective tuning parameter we selected so that when $\xi = 1$, the elongation of the waves has reached an extreme but still plausible appearance. This is inspired by a plot from [Young 1999] which showed variations of s up to 16, and it represents the only magic number in our entire system that is not based on some empirical grounding.

If $D_{\text{base}}(\omega, \theta)$ is either Mitsuyasu or Hasselmann, the product of the two functions is still a Longuet-Higgins function, with the shape parameters simply added together. This means the closed-form normalization function in equation (34) can be used. However, for the other base directional spreading functions, we have to use numerical integration to produce the denominator, which is computationally expensive. A 2D lookup table can be created as a preprocessing step to help speed this step up.

Figure 5 demonstrates the effect of the swell parameter on an ocean with otherwise identical characteristics. For zero swell, the waves are somewhat facing in the same direction, but with still a lot of chop. With swell equal to 1, the waves are strongly elongated. The swell parameter can be set to larger than 1 to elongate the waves even more.

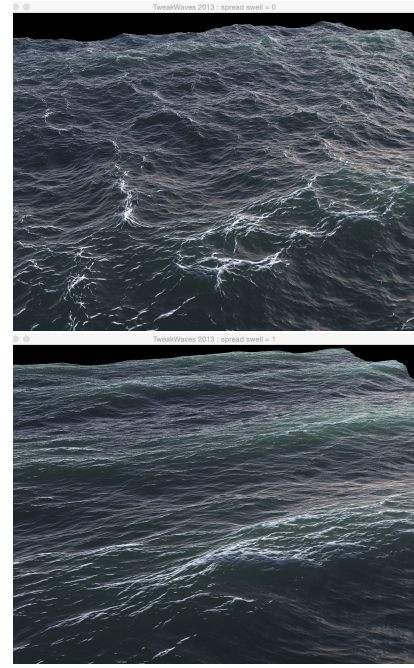


Figure 5: The same ocean with different swell amounts. From top to bottom, swell = 0, 1

7 Spectral Synthesis

For the most part, we follow the template provided by [Tessendorf 2001] when constructing our spectral initial state and propagating to a spatial state at a given time. However, we depart in a few areas that are important, which we will describe here.

7.1 Initial State

The initial state consists of two 2D arrays of complex numbers, each of which is $(N/2) + 1$ in width (in the x dimension) and N in height, where N represents the width and height of the desired spatial height field. In our system, we constrain N to be a power of two, though most FFT software can handle arbitrary sizes. When iterating in spectral space, the iteration coordinate is over discrete values of the wave vector \mathbf{k} . However, our spectra have all been written in terms of the variables (ω, θ) . To change variables correctly, the change of variables theorem has to be employed. The appendix demonstrates the details of this transformation, giving us equation (61), repeated here:

$$S(k_x, k_y) = S(\omega, \theta) \frac{d\omega}{dk} / k$$

The relationship between wave amplitude and the wave spectrum was described in equation (15), which can be solved for the mean amplitude:

$$\bar{a}(k_x, k_y, \Delta k_x \Delta k_y) = \sqrt{2S(k_x, k_y) \Delta k_x \Delta k_y} \quad (46)$$

Ocean waves in deep water are a Gaussian random process [Ochi 1998], and therefore we use a normal distribution of mean 0 and standard deviation 1 to produce a random variate $\nu_{(k_x, k_y)}$ for amplitude, which is then multiplied by \bar{a} to produce the random amplitude for wave vector \mathbf{k} :

$$a(k_x, k_y, \Delta k_x \Delta k_y) = \nu_{(k_x, k_y)} \sqrt{2S(k_x, k_y) \Delta k_x \Delta k_y} \quad (47)$$

The random value $a^2/2$ has a χ^2 distribution with 1 degree of freedom, which correctly produces a mean spectrum value of $S(k_x, k_y) \Delta k_x \Delta k_y$.

7.1.1 Random Seeding

It is common for artists to want to raise and lower the resolution of a height field and get the same ocean appearance up to the limits of the resolution. In order to create repeatability, we create pseudorandom numbers by seeding a random number generator with a hash of the wave number truncated to five digits of precision, to prevent numerical imprecision from changing the seeding.

7.1.2 Phase and Bi-Directional Waves

We use a uniform random variate distributed between $[0, 2\pi]$, seeded as above, to produce the phase of the initial state. [Tessendorf 2001] uses a single complex variate, and then uses the complex conjugate of that variate to produce waves towards and against the wave direction when propagating. This is problematic, because the waves corresponding to the negative direction, represented by wave number $-\mathbf{k} = (-k_x, -k_y)$ have a different spectrum value associated with them, and need to be handled separately. We therefore store a separate complex variate for the positive and negative waves in two separate 2D complex spectral arrays in the initial state. The negative variate is used instead of the complex conjugate when producing the time-propagated spectral state, but otherwise we follow [Tessendorf 2001].

8 Implementation

The models described in this paper are implemented in the Tweak Waves library, the source code for which is included with this paper. An OpenGL-based viewer allows for interactive exploration of the models with plausible lighting and shading, and allows us to validate our ease of use claims. We've found that ocean shaping done without a reasonably water-like shading approach will cause artists to over-sharpen their wave surfaces to compensate for perceived rounding due to the lack of the sharp fresnel effect from the water shading.

Each of the spectra and directional spreading functions is implemented in C++, and the initialization of the random spectral initial state is multithreaded using the Intel Thread Building Blocks library. Creation of a propagated state for time t is also multithreaded, and finally the inverse FFT is applied to produce the spatial fields H , DX , DY , and E as described in [Tessendorf 2001]. We apply a sharp threshold on the minimum eigenvector field E to produce a white crest map, which is seen in our example images. Artists have specifically commented on the utility of the minimum eigenvector field for the purpose of creating crest emission, blending in extra detail, and more. For a resolution of 512x512, we can adjust the ocean settings in real-time with no perceived latency on a MacBook Pro with a 2.7 GHz Intel Core i7 dual processors, 16 GB of RAM, and Intel HD Graphics 4000 with 1024 MB of graphics memory.

9 Results

Our system is easy and fast to use, and artists can match reference oceans with very little parameter tuning. Usually an artist needs only to choose the domain size, the wind speed, the ocean depth, and the swell amount to match a reference or target. Each of these parameters has a simple, intuitive meaning that requires no training to explain. The fetch parameter is easy to understand when interacting with extremely severe seas, with very high winds and ocean



Figure 6: Several views of an ocean from our model with wind speed = 25m/s, depth = 100m, spectrum = TMA, directional = Donelan-Banner, swell = 0.25, fetch = 800km.

depths. A smaller fetch of 50km will produce scattered, choppy waves, whereas a very large fetch of 1250km will produce huge, smooth, concentrated waves. A long-term goal ours has been to eliminate all of the “fudge factors” from the model implementation, in order to have confidence in the integrity of the implementation relative to these very heavily tested and validated empirical models we’re using. The last piece we were able to get correct was the change of variables determinant of the Jacobian, which seems obvious when formally written, but took a long time to understand and apply correctly. We are proud to say that with the exception of the non-empirical swell function, which contains a single magic number, our system is an exact match in every way to the spectra and spreading functions as published.

An interactive tour of the system routinely elicits joyous responses, and new users find they can drive the model with almost no explanation at all. Figure 7 shows waves produced by our model to match a photographic reference from the Wikipedia entry on Sea State http://en.wikipedia.org/wiki/Sea_state, rendered interactively in our real-time viewer. This match is quite close and aesthetically pleasing, and took only a few minutes to parameter-tune. No fudge parameters (amplitude, filtering) are used - just physical constants.

We default the system to always use the Capillary dispersion relationship, the TMA non-directional spectrum, and the Donelan-Banner directional spreading function. Our system allows the user to select alternates, but only the directional spreading ever needs to be modified in practice. The Hasselmann and Mitsuyasu variations provide interesting and useful aesthetic variation.

10 Conclusions and Future Work

We presented an in-depth adaptation of the TMA wave spectrum, and a selection of empirically-based directional spreading func-

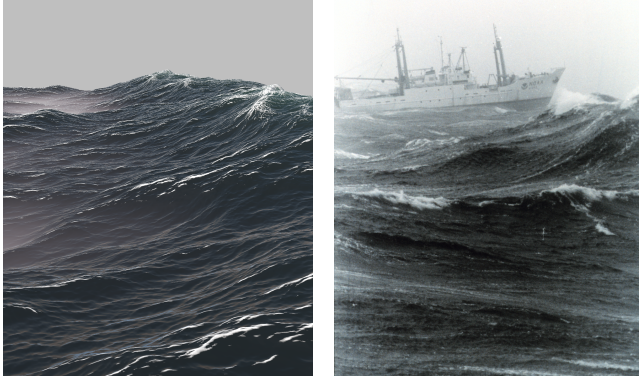


Figure 7: An ocean from our model with wind speed = 75m/s, depth = 150m, spectrum = TMA, directional = Donelan-Banner, swell = 0.35, fetch = 1250km. Shown next to NOAA photographic reference for severe sea state.

tions. We designed an intuitive, normalized function of a single parameter, “swell”, which allows for smooth blending between choppy seas and long parallel wave trains. We showed how this function can be used to modify any of the other directional spreading functions.

For future work, we’d like to get trough-damping implemented directly in the model, with a single parameter that uses the peak frequency as a normalization target. We think this would make the waves even more believable out of the box. Beyond that, the system seems to work extremely well - it is our hope that this paper will encourage use of our model and produce feedback on how it might be improved.

Acknowledgements

This paper could not have been accomplished without the patient teaching of John Anderson. Allen Hemberger, Areito Echevarria, Mike Root, and Kevin Romond provided valuable feedback on the paper, and have been longtime users upon whose experience the design of the system relied. Water is worth loving. Bill Polson at Pixar provided the insight regarding the use of the change of variables theorem when adapting the spectra to wave-number space. Shane Cooper provided valuable feedback on implementation details for early versions of this system.

Thanks to Weta Digital, Pixar Animation Studios, Google, and my colleagues from the former Tweak Films for using, supporting, and contributing to the many incarnations of Empirical Directional Waves over the last 14 years.

Allen Hemberger and Pixar Animation Studios provided beautiful rendered ocean images for this paper, and invaluable aesthetic guidance along the way. Special thanks to Bob Groothuis for the use of his Dutch Skies Sky Dome images in our interactive rendering tool.

References

- AKRAM, A., 2015. aaOcean Suite. <http://www.amaanakram.com/plugins-shaders/aaoocean-suite/>.
- BOUWS, E., E. A. 1985. Similarity of the wind wave spectrum in finite depth water, part i - spectral form. *Journal of Geophysical Research* 90, C1, 975–986.
- BOUWS, E., E. A. 1985. Similarity of the wind wave spectrum in finite depth water, part ii - quasi-equilibrium relations. *Journal of Geophysical Research*.
- COOLEY, J. W., AND TUKEY, J. W. 1965. An algorithm for the machine computation of complex fourier series. *Mathematics of Computation* 19, 297–301.
- DONELAN, M., HAMILTON, J., AND HUI, W. 1985. Directional spectra for wind-generated waves. *Phil. Trans. Roy. London A*, 315, 509–562.
- FOSTER, N., AND METAXAS, D. 1996. Realistic animation of liquids. *Graphical Models and Image Processing* 58, 5, 471–483.
- FOURIER, J. 1807. Mmoire sur la propagation de la chaleur dans les corps solides. *Nouveau Bulletin des sciences par la Socit philomatique de Paris I*, 6, 112116.
- FOURNIER, A., AND REEVES, W. T. 1986. A simple model of ocean waves. In *ACM Trans. Graph. (Proc. of SIGGRAPH)*, vol. 20, 75–84.
- FRIGO, M., AND JOHNSON, S. G. 2005. The design and implementation of FFTW3. *Proceedings of IEEE* 93, 2, 216–231.
- HASSELMANN, K., BARNETT, T., BOUWS, E., CARLSON, H., CARTWRIGHT, D., ENKE, K., EWING, J., GIENAPP, H., HASSELMANN, D., KRUSEMAN, P., MEERBURG, A., MUELLER, P., OLBERS, D., RICHTER, K., SELL, W., AND WALDEN, H. 1973. Measurements of wind-wave growth and swell decay during the joint north sea wave project (JONSWAP). *Ergnzungsheft zur Deutschen Hydrographischen Zeitschrift Reihe* 8, 12, 95.
- HOLTHUIJSEN, L. H. 2007. *Waves in Oceanic and Coastal Waters*. Cambridge University Press.
- HUGHES, S. A. 1984. The TMA shallow-water spectrum description and applications. Technical report.
- KASS, M., AND MILLER, G. 1990. Rapid, stable fluid dynamics for computer graphics. In *ACM Trans. Graph. (Proc. of SIGGRAPH)*, vol. 24, 49–57.
- KITAIGORODSKII, S., KRASITSKII, V., AND ZASLAVSKII, M. 1975. On phillips’ theory of equilibrium range in the spectra of wind-generated gravity waves. *Physical Oceanography* 13, 5, 816–827.
- LEE, N., BAEK, N., AND RYU, K. W. 2008. A real-time method for ocean surface simulation using the tma model. *International Journal of Computer Information Systems and Industrial Management Applications (IJCISIM)*.
- LONGUET-HIGGINS, M., CARTWRIGHT, D., AND SMITH, N. 1961. Observations of the directional spectrum of sea waves using the motions of a floating buoy. *Proceedings of the Conference of Ocean Wave Spectra*, 111–132.
- MITSUYASU, H. E. A. 1975. Observations of the directional spectrum of ocean waves using a clover-leaf buoy. *Journal of Physical Oceanography* 5, 750–760.
- NIELSEN, M., AND BRIDSON, R. 2011. Guide shapes for high resolution naturalistic liquid simulation. In *ACM Transactions on Graphics (Proceedings of ACM SIGGRAPH)*, vol. 30, 831–838.
- NIELSEN, M. B., SÖDERSTRÖM, A., AND BRIDSON, R. 2013. Synthesizing waves from animated height fields. *ACM Trans. Graph.* 32, 1 (Feb.), 2:1–2:9.

- OCHI, M. K. 1998. *Ocean Waves*. Cambridge University Press.
- PHILLIPS, O. M. 1958. The equilibrium range in the spectrum of wind-generated ocean waves. *Journal of Fluid Mechanics* 4, 426–434.
- PIERSON, W. J., AND MOSKOWITZ, L. 1964. A proposed spectral form for fully developed windseas based on the similarity theory of s. a. kitaigorodskii. *Journal of Geophysical Research* 69, 5181–5190.
- PIERSON, W. J. J., NEUMANN, G., AND JAMES, R. W. 1954. *Practical Methods for Observing and Forecasting Ocean Waves by means of Wave Spectra and Statistics*.
- READ, P., 2009. Fluids notes. <http://www.atm.ox.ac.uk/user/read/fluids/fluidsnote5.pdf>.
- STAM, J. 2002. A simple fluid solver based on the fft. 43–52.
- STEWART, R. 2008. *Introduction to Physical Oceanography*.
- TESSENDORF, J. 2001. Simulating ocean water. White paper.
- THOMPSON, E. F., AND VINCENT, C. L. 1983. Prediction of wave height in shallow water. *Proceedings of Coastal Structures 1983, American Society of Civil Engineers*, 1000–1008.
- WEN, S.-C., GUO, P.-F., AND ZHANG, D.-C. 1993. Analytically derived wind-wave directional spectrum : Parts 1&2. *Journal of Oceanography* 49, 131–147.
- YOUNG, I. 1999. *Wind Generated Ocean Waves*. Elsevier.

Appendix A: Wave Vector Spectrum, Change of Variables

The wave spectrum $S(\omega, \theta)$ is defined in terms of the variables ω, θ , but the spectral field we create for the Inverse FFT is discretized in terms of the wave vector \mathbf{k} 's components, k_x, k_y . Each 2D spectral point evaluates a discrete approximation of the integral of the spectrum over a region of constant size $\Delta k_x, \Delta k_y$. The integral of the spectrum over a small interval $\Delta\omega, \Delta\theta$ in frequency and angle space is used to calculate the time-average of wave energy for that small set of waves, as described in equation (13). In order to integrate with the substituted variables k_x, k_y , we must employ the change of variables theorem, which, adapted to this problem space, states:

$$\int_{\omega(k_x, k_y)} \int_{\theta(k_x, k_y)} S(\omega(k_x, k_y), \theta(k_x, k_y)) d\omega d\theta = \int_{k_x} \int_{k_y} S(k_x, k_y) |\det(J_{\omega, \theta})| dk_x dk_y \quad (48)$$

Where $|\det(J_{\omega, \theta})|$ represents the absolute value of the determinant of the Jacobian matrix containing the partial derivatives of ω, θ with respect to k_x, k_y :

$$|\det(J_{\omega, \theta})| = \left\| \begin{array}{cc} \frac{\partial \omega}{\partial k_x} & \frac{\partial \omega}{\partial k_y} \\ \frac{\partial \theta}{\partial k_x} & \frac{\partial \theta}{\partial k_y} \end{array} \right\| = \left| \frac{\partial \omega}{\partial k_x} \frac{\partial \theta}{\partial k_y} - \frac{\partial \omega}{\partial k_y} \frac{\partial \theta}{\partial k_x} \right| \quad (49)$$

Given the magnitude of the wave vector:

$$k = \sqrt{k_x^2 + k_y^2} \quad (50)$$

and the relationship between ω and k given by any dispersion relation:

$$\omega = \phi(k) \quad (51)$$

We can use the chain rule to calculate the partial derivatives, which are as follows:

$$\frac{\partial \omega}{\partial k_x} = \frac{d\phi(k)}{dk} \frac{k_x}{k} \quad (52)$$

$$\frac{\partial \omega}{\partial k_y} = \frac{d\phi(k)}{dk} \frac{k_y}{k} \quad (53)$$

$$\frac{\partial \theta}{\partial k_x} = -\frac{k_y}{k^2} \quad (54)$$

$$\frac{\partial \theta}{\partial k_y} = \frac{k_x}{k^2} \quad (55)$$

Substituting the above equations into the absolute value of the determinant of the Jacobian from (49), we get:

$$|\det(J_{\omega, \theta})| = \left| \frac{d\phi(k)}{dk} / k \right| \quad (56)$$

We can therefore express the differential change of variables as:

$$d\omega d\theta = \left| \frac{d\phi(k)}{dk} / k \right| dk_x dk_y \quad (57)$$

The discrete approximation is:

$$\Delta\omega \Delta\theta \approx \left| \frac{d\phi(k)}{dk} / k \right| \Delta k_x \Delta k_y \quad (58)$$

Finally, this can be substituted into the formula for mean amplitude from equation (15), using the definitions of ω and k from equations (50) and (51):

$$\bar{a}(k_x, k_y, \Delta k_x, \Delta k_y) = \sqrt{2S(\omega, \theta) \left| \frac{d\phi(k)}{dk} / k \right| \Delta k_x \Delta k_y} \quad (59)$$

In [Ochi 1998], Section 2.1.6 describes the relationship between the wave frequency spectrum and the wave number spectrum. His equation 2.8 is for a single directional angle only, and is given as:

$$S(k) = S(\omega) \frac{d\omega}{dk} \quad (60)$$

By the derivation above, we can state that for the full directional spectrum,

$$S(k_x, k_y) = S(\omega, \theta) \frac{d\omega}{dk} / k \quad (61)$$

For the full dispersion relationship given in (9), the derivative with respect to the wave number k is:

$$\frac{d\phi(k)}{dk} = \frac{h(\frac{\sigma}{\rho} k^3 + gk) \operatorname{sech}^2(hk) + \phi(k)^2}{2\phi(k)} \quad (62)$$